Angle-resolved photoemission study of the rare-earth intermetallic compounds: $R\mathrm{Ni}_2\mathrm{Ge}_2$ (R=Eu, Gd)

J. Park, D. P. Brammeier, C. G. Olson, P. C. Canfield, and D. W. Lynch
Department of Physics and Astronomy and Ames Laboratory, U.S. Department of Energy, Iowa State University, Ames, Iowa 50011, USA
(Received 5 April 2004; published 18 August 2004)

Experimental energy bands mapped from normal-emission photoelectron spectra of $EuNi_2Ge_2$ and $GdNi_2Ge_2(001)$ surfaces show four photoemission features that disperse in both materials in good agreement with band calculations. Segments of the Fermi surfaces mapped by angle-resolved photoemission spectroscopy in the ΓXPZ plane of the Brillouin zones for both $EuNi_2Ge_2$ and $GdNi_2Ge_2$ are in good agreement with band calculations. This Fermi surface segment changes when one electron is added to $EuNi_2Ge_2$, corresponding to $GdNi_2Ge_2$, based on the rigid-band approximation.

DOI: 10.1103/PhysRevB.70.075105 PACS number(s): 71.20.Eh, 71.20.Lp, 79.60.−i

I. INTRODUCTION

$EuNi_2Ge_2$ and $GdNi_2Ge_2$ are two members of the RT_2X_2 (R=rare earth, T=transition metal, and X=Si, Ge) family of the ternary rare-earth intermetallic compounds, studied since the early 1980s. Extensive studies of the RT_2X_2 with their wide variety of magnetic properties can be found in Refs.1–3. The magnetic properties of the rare-earth nickel germanides $R\mathrm{Ni}_2\mathrm{Ge}_2$ were recently studied in more detail.[4] Their long-range magnetic order can be explained by the indirect Ruderman-Kittel-Kasuya-Yosida (RKKY) exchange interaction between the magnetic rare-earth ions through the conduction electrons.[5,6] Magnetic measurements have revealed that the Eu ion in $EuNi_2Ge_2$ has an $^8S_{7/2}$ ground state with an effective magnetic moment $\mu_{eff}\sim 7.7\ \mu_B$, indicating that Eu is divalent with the $4f^7$ electron configuration in the ground state. $EuNi_2Ge_2$ is antiferromagnetic (AF) below its Néel temperature (T_N) of 30.8 K.[4] The temperature-dependent magnetic susceptibility of $GdNi_2Ge_2$ shows $\mu_{eff}\sim 8.0\ \mu_B$, close to the theoretical value of 7.9 μ_B for the free Gd^{3+} ion, with the same stable $4f^7$ ($^8S_{7/2}$) ground state as Eu in $EuNi_2Ge_2$. $GdNi_2Ge_2$ has a transition to an AF state at a T_N of 27.1 K.[4] The valence is consistent with our photoelectron spectra of the $4f$ states for both materials (not shown). Eu is indeed divalent and Gd is trivalent in these compounds.

From Mössbauer spectra[7] the easy axis of magnetization is at an angle of 44°, and close to 75°, from the c axis for $EuNi_2Ge_2$ and $GdNi_2Ge_2$ polycrystalline samples, respectively, below T_N. Both materials have second transition temperatures below T_N. In $EuNi_2Ge_2$ a second transition (T_t) occurs at 13.4 K and T_t is 16.8 K in $GdNi_2Ge_2$. It is suggested for both single crystals that the ordered magnetic moments below T_N are in the basal plane (a-b plane), and in the case of $GdNi_2Ge_2$, between T_t and T_N there is an ordered component of the moment along the c axis from temperature-dependent magnetic susceptibility measurements.[8]

The AF Néel transition is reported to be driven by strong Fermi-surface nesting from x-ray resonant exchange scattering.[8] These nestings of $EuNi_2Ge_2$ and $GdNi_2Ge_2$ are responsible for the modulations of $\mathbf{q}_{\mathrm{nest}}=(0,0,q_z)$ with $q_z=1$ and 0.79, respectively. A generalized susceptibility calculation using the self-consistent tight-binding linear muffin-tin orbital (TBLMTO) method[9–11] showed that Fermi-surface nesting is responsible for the magnetic structure. $EuNi_2Ge_2$ is isostructural to $GdNi_2Ge_2$, in which Gd has a valence of 3 + with one more conduction electron than Eu in $EuNi_2Ge_2$. Therefore these compounds, which have the same Hund's rule ground state ($^8S_{7/2}$), are suitable systems for the quantitative study of band filling effects on electronic structure. This is due to the fact that the band structure and total density of states (DOS) in $EuNi_2Ge_2$ and $GdNi_2Ge_2$ are so similar qualitatively, but the Fermi energy (E_F) of $GdNi_2Ge_2$ is higher due to increased band filling,[8] which suggests that a rigid-band model is adequate as a first-order approximation in the electronic structure. The purpose of this paper is to investigate the electronic structure of the valence bands of $EuNi_2Ge_2$ and $GdNi_2Ge_2$ single crystals and to check the assumptions that the f electrons are noninteracting and, consequently, the rigid-band model for these crystals would work.[8] First, the electronic band structure of $EuNi_2Ge_2$ and $GdNi_2Ge_2$ along the $\Gamma-Z$ [001] direction in the bulk Brillouin zone (BZ) was determined by taking normal-emission photoelectron spectra and comparing the experimental results to the theoretical ones. We studied quantitatively the effects of band filling on the electronic structures by observing a rigid-band shift of E_F simply corresponding to an increase of one electron ($1e$/atom) upon going from $EuNi_2Ge_2$ to $GdNi_2Ge_2$. Then, we performed angle-resolved photoemission spectroscopy (ARPES) experiments and compared the experimental results to band structure calculations, confirming again the effects of band filling on electronic structures.

II. EXPERIMENT

$EuNi_2Ge_2$ and $GdNi_2Ge_2$ crystallize in the $ThCr_2Si_2$ structure (space group $I4/mmm$), with a body-centered-tetragonal (bct) lattice. The corresponding simple tetragonal unit cell is shown in Fig. 1. The experimental lattice parameters are $c=10.10$ Å and $a=4.14$ Å for $EuNi_2Ge_2$, and $c=9.783$ Å and $a=4.063$ Å for $GdNi_2Ge_2$.[12] Single crystals were grown using a high-temperature-solution-growth technique.[13]

All photoemission experiments were carried out at the Ames/Montana ERG/Seya beam-line[14] at the Synchrotron

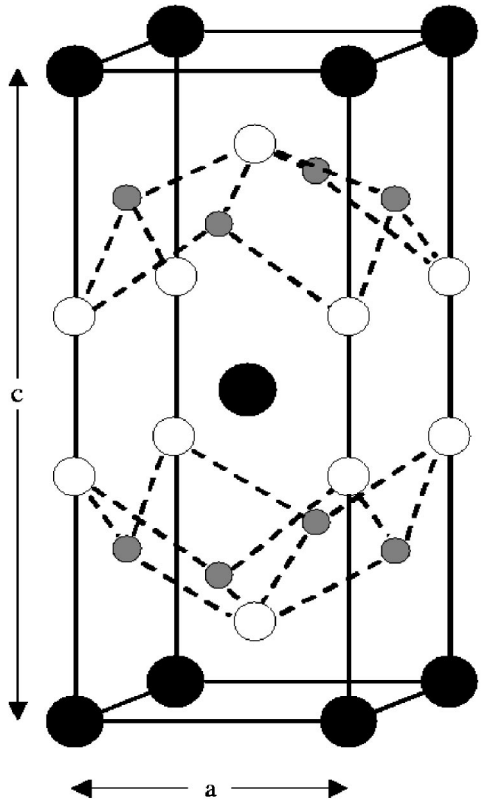

FIG. 1. Crystal structure of $EuNi_2Ge_2$ and $GdNi_2Ge_2$. Eu or Gd, Ni, and Ge atoms are represented by large filled circles, small shaded circles, and the white circles respectively.

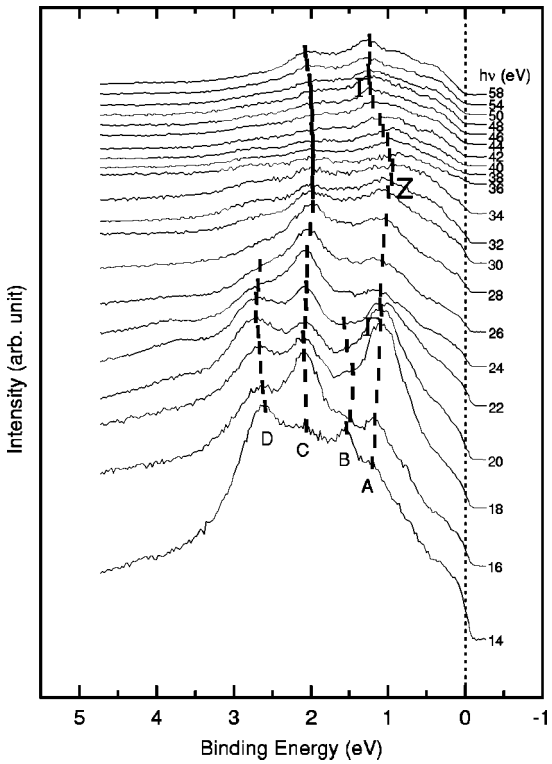

FIG. 2. EDCs for $EuNi_2Ge_2$ at normal emission from the (001) surface (Γ-Z direction) taken with increasing photon energy. Binding energies (BEs) are referenced to the Fermi energy (E_F) and the spectra have been arbitrarily displaced along the ordinate for clarity. The vertical bars are a guide to the eye which qualitatively follow the major features of the scans.

Radiation Center, Stoughton, Wisconsin. The samples were cleaved *in situ* at a pressure below 3×10^{-11} Torr, and temperature below 20 K. The clean surfaces were (001) planes. The overall energy resolution of the experiment, determined from the Fermi edge of a sputtered Pt foil, was about 50 meV at $h\nu\sim22$ eV and 145 meV at $h\nu\sim70$ eV. The analyzer input lens had an angular acceptance of 2°, about 6% of the distance from Γ to X in the Brillouin zone. The Fermi energy (E_F) of the system was calibrated from the valence-band spectrum of a freshly sputtered Pt foil in electrical and thermal contact with samples. The angle of incidence of the *p*-polarized photons was ~40° with respect to the sample surface normal. The sample alignment was determined in situ by using the symmetry of the dispersion of spectral features at high-symmetry points.

III. RESULTS AND DISCUSSION

Figure 2 shows photoelectron energy distribution curves (EDCs) for $EuNi_2Ge_2$ taken at normal emission from an (001) surface with a range of photon energies ($h\nu's$). The four dispersing features are a feature around 1 eV (A), a weak feature around 1.5 eV (B), another around 2 eV (C), and a feature around 2.5 eV (D). Feature A exhibits significant energy dispersion with changing $h\nu$ over an energy range of nearly 0.38 eV, from its deepest value of 1.28 eV binding energy (BE) at $h\nu=48$ eV to its smallest value, 0.90 eV at $h\nu=33$ eV. One set of peaks, labeled C, appears at an almost fixed BE of around 2 eV, independent of the incident photon energy, which shows that any dispersion is small. This is expected from *d*-character bands, which dominate this region of the valence band. Feature D disperses as the photon energy is changed from 14 to 26 eV, clearly showing a BE shift between 2.6 and 2.8 eV. At higher photon energies ($h\nu>30$ eV), we found small dispersion for features B and D, although the peak intensity is low. Dispersion might be masked by strong intensity modulations due to matrix-element effects if the features are composite in nature.

Figure 3 presents similar spectra for $GdNi_2Ge_2$. There are four features which exactly correspond to those of $EuNi_2Ge_2$, at around 1.2 eV (A), a weak feature around 1.8 eV (B), another around 2.2 eV (C), and one around 2.8 eV (D). It is notable that all features for $GdNi_2Ge_2$ are at about 0.25 eV lower BE than those of $EuNi_2Ge_2$. Feature A disperses from its deepest value of 1.30 eV at $h\nu=22$ eV to its smallest value of 1.25 eV at $h\nu=32$ eV. Feature D disperses as the photon energy is changed from 14 to 2.2 eV. Looking again at feature A in both materials, we see that it disperses at almost all photon energies. There is some symmetry as it curves towards and away from E_F. This is required by crystal periodicity and can be used as a cross-check in band dispersions of complicated systems.[15] The dispersions in Figs. 2 and 3 are strong enough that we were able to map them through k space and look for symmetry points. The high

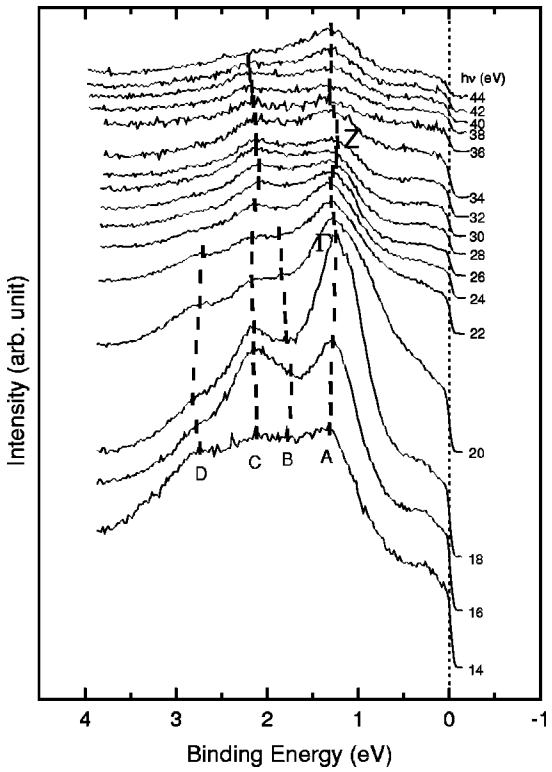

FIG. 3. EDCs for $GdNi_2Ge_2$ at normal emission from the (001) surface (Γ-Z direction) taken with increasing photon energy from 14 to 44 eV.

symmetry points, Γ and Z, are indicated to the right and left of feature A in Figs. 2 and 3.

Inside the crystal the electronic potential is approximated according to the muffin-tin model, i.e., spherically symmetric potentials around each atom and a constant potential in between.[16] Assuming the free electronlike final-state model[17] in a constant positive inner potential (V_0), the external measured kinetic energy (E_{kin}) and the internal final-state wave vector ($\mathbf{k}_f$) are related by

$$E_{\mathrm{kin}} = \frac{\hbar^2 \mathbf{k}_f^2}{2m} - (V_0 + \Phi) \tag{1}$$

$$= \frac{\hbar^2 (k_{f\perp}^2 + k_{f\parallel}^2)}{2m} - (V_0 + \Phi), \tag{2}$$

where m is the mass of the electron and Φ is work function of the sample and V_0 is referenced to E_F which defines the zero of the free-electron-final-state band. $E_F - V_0$ is approximately the filled valence bandwidth. Since the component of momentum parallel to the surface ($k_{f\parallel}$) is zero in normal emission, $k_{f\perp}$, the momentum perpendicular to the surface (001), is to be evaluated. This approach is useful when the photon energy is above about 30 eV, so that a free-electron final state is a reasonable approximation. The work function Φ was set to $\Phi = 4.3$ eV and V_0 is to be determined. In fact, the actual work function barrier seen by a photoelectron is the work function of the electron analyzer since the sample is in electrical contact with the energy analyzer but we assumed that it is very close to that of the sample itself. Going beyond the Z point at the zone boundary, the peak reverses its dispersion and traces its way back to the Γ point in the next Brillouin zone. This symmetric behavior of the dispersion around Γ and Z can be used to determine the value of V_0 by adjusting V_0 to make $k_{f\perp}$ fit the dispersion of repeating band feature A. The values of V_0 for $EuNi_2Ge_2$ and $GdNi_2Ge_2$ were estimated to be 11.0 ± 0.2 and 11.5 ± 0.2 eV by using a direct-transition model and assuming a free-electron band structure. They are excellent agreement with the bottoms of the free-electron-like bands (10.95 and 11.48 eV, respectively) in the band structures in Ref. 18.

We compare the experimentally measured band dispersions of $EuNi_2Ge_2$ and $GdNi_2Ge_2$ with the theoretical band structure calculations along the Γ-Z direction performed by Islam[18] in Fig. 4. A few bands were not observed because certain transitions can be forbidden by symmetry selection rules. The band dispersions of $EuNi_2Ge_2$ appear to be consistent with the theoretical calculations, but compared with

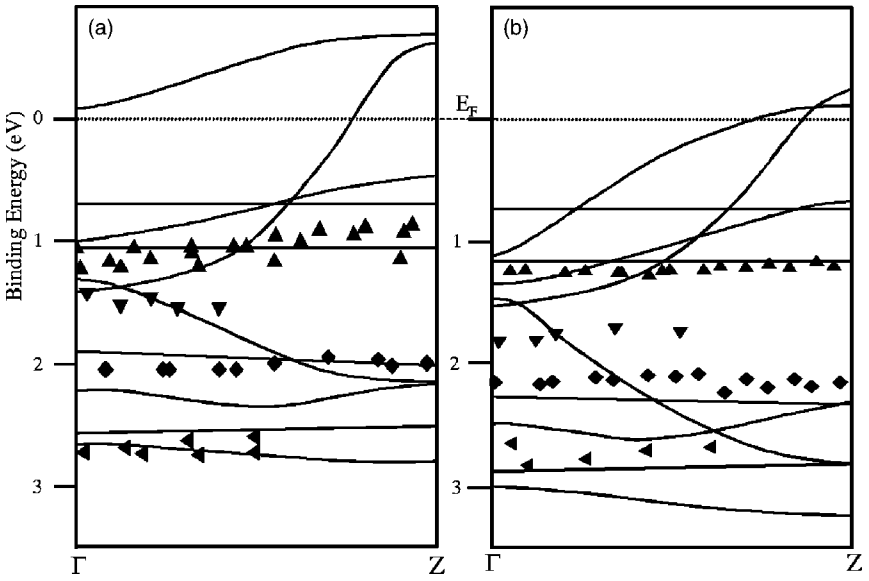

FIG. 4. The measured band dispersion of (a) $EuNi_2Ge_2$ and (b) $GdNi_2Ge_2$ along the Γ-Z [001] direction in comparison with the band structure calculations in Ref. 18 (full curves). Symbols show the observed direct-transition features: A (triangle), B (inverted triangle), C (diamond), and D (leftward triangle). The dotted horizontal line is the Fermi level; the solid horizontal lines are $4f$ bands.

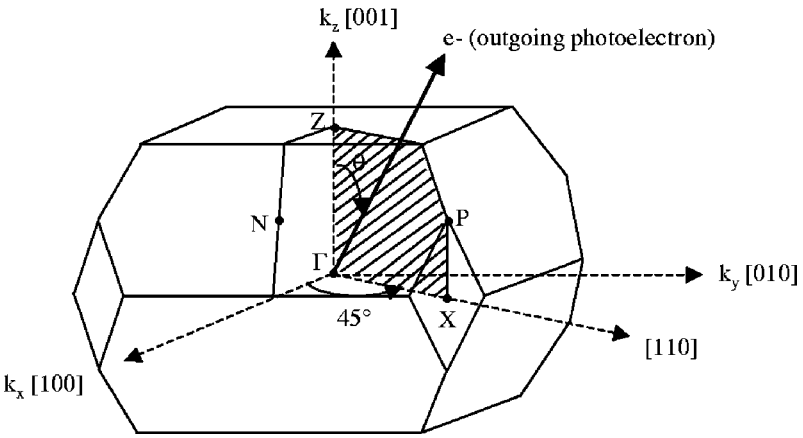

FIG. 5. Brillouin zone for a body centered tetragonal structure. The high-symmetry ΓXPZ plane used in our ARPES is hatched.

the band structure calculation there is a rigid downward shift of the experimentally determined band structure. According to Ref. 18, Islam calculated the generalized electric susceptibility $\chi_0(q)$ by shifting the E_F upward by 10 mRyd (to E_F' $=E_F+0.136$ eV) for $EuNi_2Ge_2$ and 7 mRyd (to $E_F''=E_F$ $+0.095$ eV) for $GdNi_2Ge_2$ in order to adjust his nesting vectors. He pointed out that such a shift is not unreasonable for band calculations using the atomic-sphere approximation (ASA), when multiple bands with different orbital characters cross E_F. The experimental band structure of $EuNi_2Ge_2$ fits apparently much better with the theoretical band calculation when E_F is shifted up by ~ 0.136 eV. Therefore it seems true that it often is found necessary to shift the position of E_F within the accuracy of the electron energies, 1% of the *s*, *p*, and *d* bandwidths,[10] to align the experimental band structure with those of LMTO ASA calculations. Those of $GdNi_2Ge_2$ are shown in Fig. 4(b) as well. But for $GdNi_2Ge_2$, experimental photoemission data show a little better agreement with the original band structure rather than one with a Fermi-level shift of 0.095 eV upward.

Theoretically, the addition of exactly "one" electron ($1e$/atom) was obtained from the DOS of $EuNi_2Ge_2$ based on the rigid-band approximation. This has the effect of lifting the E_F of $EuNi_2Ge_2$ by ~ 0.3 eV.[8] Our results for $GdNi_2Ge_2$ show that all of the observed band features have higher BEs by 0.2 to 0.3 eV compared to those of $EuNi_2Ge_2$. Therefore the observed BE shift can be interpreted quantitatively by a rigid-band shift of E_F based on the rigid-band model as a first approximation, although a rigid-band description has been shown to be unsuccessful for some electronic states of alloys from photoemission investigations.[19,20] Our present results are also consistent with the interpretation by Islam *et al.*,[8] in which the E_F shift simply corresponds to an increase of one electron per rare-earth atom upon going from $EuNi_2Ge_2$ to $GdNi_2Ge_2$. In fact, the lattice parameters of $EuNi_2Ge_2$ are 3% larger than those of $GdNi_2Ge_2$ due to the larger ionic radius of divalent Eu but it is assumed that it does not affect rigid-band filling much. Ignoring the difference of lattice parameters in both materials was previously supported by Islam,[8] who repeated generalized susceptibility $\chi_0(q)$ calculations by swapping the lattice constants between two compounds and found no significant changes. In the electronic band calculation, the Eu $4f$ and Gd $4f$ electrons were treated as part of the atomic cores and it is assumed that their paramagnetic bands will be similar to those of $EuNi_2Ge_2$ and $GdNi_2Ge_2$. Therefore the bct BZ is used in the analysis of the photoemission spectra rather than those corresponding to the perfect AF state. From our results it is also justified that the Eu $4f$ and Gd $4f$ electrons can be treated as core electrons in the band calculations.

Figure 5 shows the BZ of the bct structure with symmetry points labeled. The ΓXPZ plane on which we performed ARPES is shown hatched with the photoelectron emission angle θ indicated. The $k_\parallel$ component of the photoelectrons is along the[110] direction, as shown.

Figure 6 shows a set of angle-resolved EDCs from $EuNi_2Ge_2$ taken with $h\nu$s of (a) 24 eV and (b) 29 eV from an (001) surface while changing the angle in the[110] direction (in the ΓXPZ plane). The photoelectron-emission angles relative to the surface normal θ are marked next to each curve. All features show, upon decreasing the collection angle, a peak that sharpens somewhat upon approaching E_F, then drops as the initial states cross E_F. Since photoemission only measures occupied electronic states, this signifies that the initial state passed through E_F.[21,22] It can be seen that all bands disperse toward E_F on going from higher to lower angles as indicated in Figs. 6(a) and 6(b). From Fig. 6, the E_F crossing is at 20° for $h\nu=24$ eV and 18° for $h\nu=29$ eV. Each gives a point in a BZ lying on a FS.

Similar angle-resolved EDCs from $GdNi_2Ge_2$ taken with each photon energy from an (001) surface at k points in the ΓXPZ plane are shown in Fig. 7. The dispersing peak of Fig. 6 is not evident, even in plots of energy derivatives of the smoothed spectra. This was the best of several surfaces measured, but it was not as good as that of $EuNi_2Ge_2$. In order to map part of the Fermi surface of $GdNi_2Ge_2$ we plotted the step height at the Fermi edge vs collection angle for each photon energy. For $EuNi_2Ge_2$ there was a drop-off of about 20% at the same angles at which the dispersing peak was judged to be crossing the Fermi level. For $GdNi_2Ge_2$ the drop-offs were smaller, about 8%, except at 30 eV. At this energy the fall-off was either at the largest angle used, or a still larger angle, so only a lower limit to $k_{f\parallel}$ at E_F can be obtained. These results were unchanged when the normalization point in the spectra was changed.

Figure 8 shows cuts through the extended BZs of $EuNi_2Ge_2$, $GdNi_2Ge_2$, and the location of the FS crossing at different points mapped onto the ΓXPZ plane. The vertical axis is $k_\perp$ relative to the (001) surface. The horizontal axis $k_{f\parallel}$

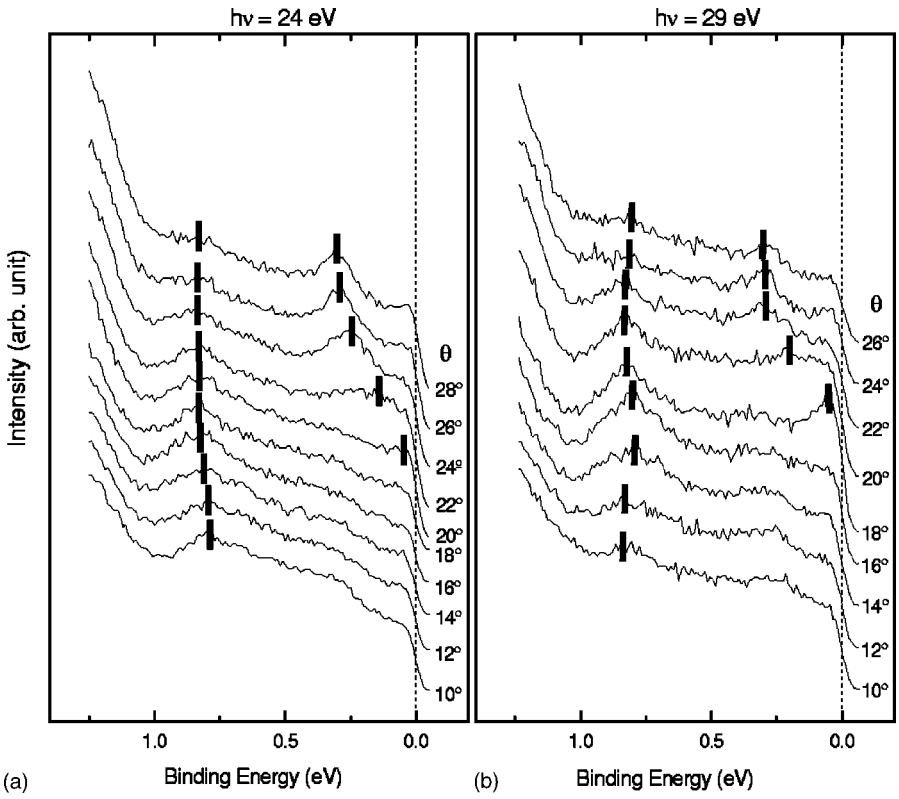

FIG. 6. A set of angle-resolved EDCs from $EuNi_2Ge_2$ taken with photon energies ($h\nu$'s) of (a) 24 eV and (b) 29 eV from a (001) surface at k points in the ΓXPZ plane. (θ is the emission angle from the sample normal.) The vertical bars are a guide to the eye which qualitatively follow the major features of the scans.

is the momentum parallel to the [110] direction. If an electron of E_{kin} with a fixed θ from the surface normal is detected, the location of the internal final-state wave vector ($\mathbf{k}_f$) is restricted to a certain circle in k space. As the electron analyzer angle is varied at a fixed photon energy, a circular k-space arc is traversed.[23,24] As shown in Fig. 8(a) the circular paths, composed of dots in the ΓXPZ plane of the BZ of $EuNi_2Ge_2$ for $V_0 \sim 11.0$ eV, are contours for various constant photon energies for initial states near E_F, assuming free-electron final states. The filled circles represent E_F crossing points, each determined from one set of curves. They are part of the hole surface around Γ in the BZ, indicating that the occupied electronic states are in the right-hand part of the ΓXPZ plane of $EuNi_2Ge_2$. We see then that the FS forms an open orbit along the c axis. The curved line is from the band calculation from Ref. 18. In fact, two bands cross along Γ-X but only the band crossing nearest to X is observed. There is a close correspondence of the theoretical and experimental FS.

The locations of the E_F crossings at different points mapped onto the ΓXPZ plane of $GdNi_2Ge_2$ are shown in Fig. 8(b). Again, the right-hand part of the ΓXPZ plane of $GdNi_2Ge_2$ contains the occupied electronic states. Compared to the FS of $EuNi_2Ge_2$, that of $GdNi_2Ge_2$ has a bulge toward the Γ point, due to the extra conduction electron from the Gd^{3+} ion, confirming again the effects of rigid-band filling on electronic structures together with the previous data on the energy band mappings. Thus a simple rigid-band model offers a way to estimate the amount of E_F variation, corresponding to an increase of exactly "one" electron in $EuNi_2Ge_2$, upon going from $EuNi_2Ge_2$ to $GdNi_2Ge_2$. One future experiment might be to do ARPES on $Gd_xEu_{1-x}Ni_2Ge_2$ pseudoternary alloys to study gradual band-filling effects in detail. Changing the stoichiometry of these pseudoternary alloys would permit observation of gradual changes in the FSs and the evolution of the electronic band structure with increasing Gd concentration.

IV. CONCLUSIONS

The electronic structures of $EuNi_2Ge_2$ and $GdNi_2Ge_2$ have been investigated using photoemission spectroscopy, via energy bands mapped from the normal-emission spectra of $EuNi_2Ge_2$ and $GdNi_2Ge_2(001)$ surfaces. Four major photoemission features dispersing along the normal [001] BZ direction in both materials are in good agreement with earlier band calculations. Our results for $GdNi_2Ge_2$ show that all of the observed band features are shifted downward by 0.2 to 0.3 eV compared to those of $EuNi_2Ge_2$, corresponding to an increase of one electron ($1e$/atom) in $GdNi_2Ge_2$ upon going from $EuNi_2Ge_2$ to $GdNi_2Ge_2$. The FSs mapped by ARPES in the ΓXPZ planes of the BZs for both materials were in good agreement with those from band structure calculations. $EuNi_2Ge_2$ is isostructural to $GdNi_2Ge_2$, but its conduction band has one less electron. Compared to the FSs of $EuNi_2Ge_2$ in the ΓXPZ plane of the BZ, $GdNi_2Ge_2$ has a bulge toward the Γ point, indicating that E_F is located at a higher energy than that of $EuNi_2Ge_2$. It can also be said that the FS will shrink toward the X point in the ΓXPZ planes when electrons are removed in $GdNi_2Ge_2$. Therefore those compounds which give the same Hund's rule ground state ($^8S_{7/2}$) were an ideal system for the study of effects of band filling on electronic structures.

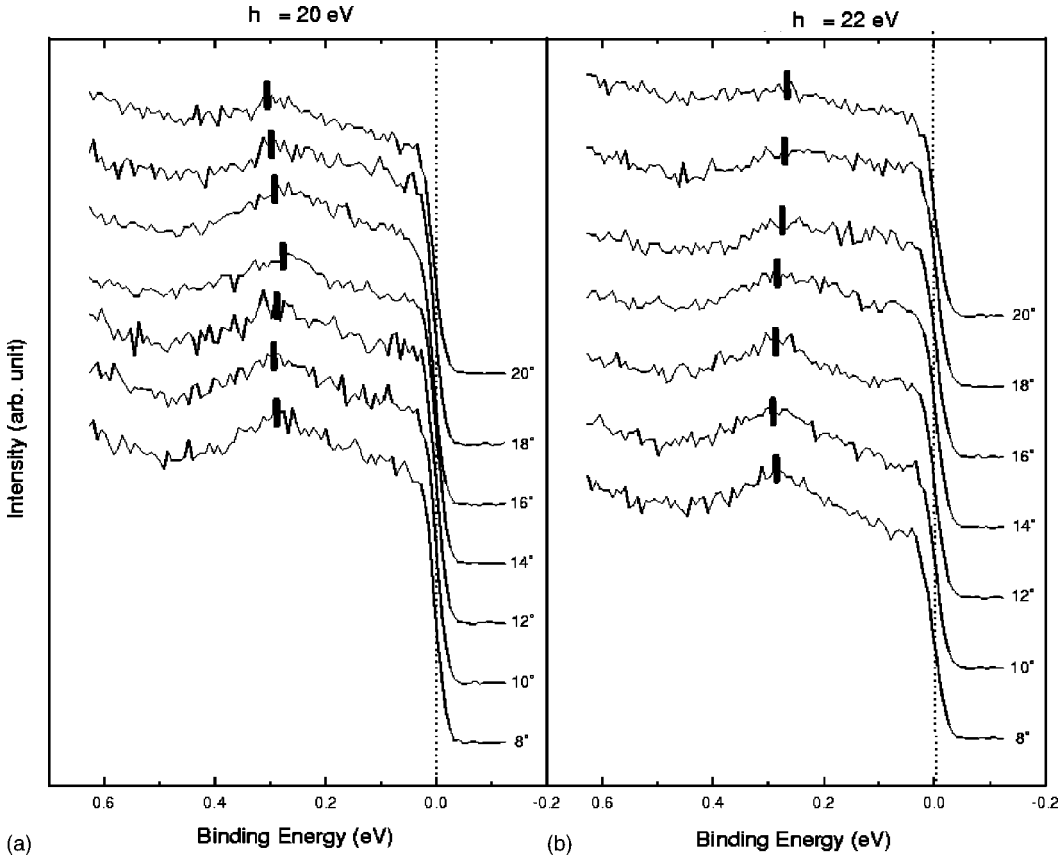

FIG. 7. The angle-resolved EDCs from $GdNi_2Ge_2$ taken with photon energies of (a) 20 eV and (b) 22 eV from a (001) surface at k points in the ΓXPZ plane. (θ is the emission angle from the sample normal.) Vertical bars following the features are included to help guide the eye.

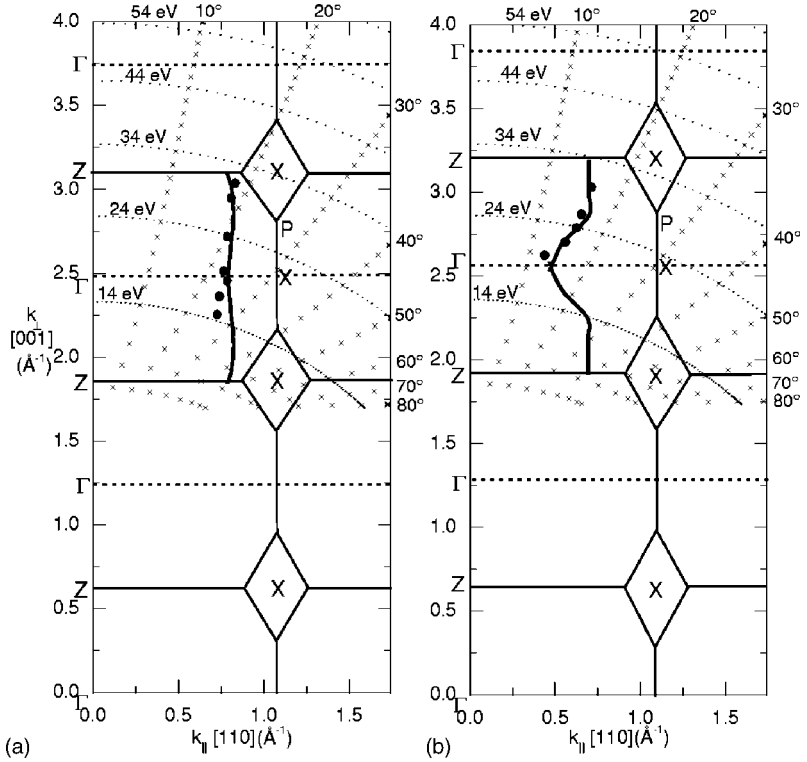

FIG. 8. Fermi surfaces (FSs) mapped in the ΓXPZ plane of (a) $EuNi_2Ge_2$ and (b) $GdNi_2Ge_2$ using an extended zone scheme. Dotted circular arcs through the BZ relate $k_\perp$ to $k_{f\|}$ at constant photon energy for initial states near E_F. The k locations for observable transitions at fixed collection angles are along the paths marked with crosses. Filled circles indicate the experimental data. The solid line indicates the theoretical FS of $EuNi_2Ge_2$ and $GdNi_2Ge_2$ by Ref. 18.

ACKNOWLEDGMENTS

We are grateful to Dr. Zahirul Islam for helpful discussions. The Ames Laboratory is operated for the U. S. Department of Energy by Iowa State University under Contract No. W-7405-ENG-82. This work was supported by the Director for Energy Research, Office of Basic Energy Science. The Synchrotron Radiation Center, University of Wisconsin-Madison, is supported by the NSF under Grant No. DMR-0084402.

[1] H. Pinto, M. Melamud, M. Kuznietz, and H. Shaked, Phys. Rev. B **31**, 508 (1985).
[2] A. Szytuła and J. Leciejewicz, in *Handbook on the Physics and Chemistry of Rare Earths*, edited by K. A. Gschneidner, Jr. and L. R. Eyring (North-Holland, Amsterdam, 1989), Vol. 12, Chap. 83.
[3] A. Szytuła and J. Leciejewicz, *Handbook of Crystal Structures and Magnetic Properties of Rare Earth Intermetallics* (CRC Press, Boca Raton, 1994), pp. 114–192.
[4] S. L. Bud'ko, Z. Islam, T. A. Wiener, I. R. Fisher, A. H. Lacerda, and P. C. Canfield, J. Magn. Magn. Mater. **205**, 53 (1999).
[5] R. J. Elliott, in *Magnetism*, edited by G. T. Rado and H. Suhl (Academic Press, New York, 1965), Vol. IIA, Chap. 7.
[6] S. H. Liu, in *Handbook on the Physics and Chemistry of Rare Earths*, edited by K. A. Gschneidner, Jr. and L. R. Eyring (North-Holland, Amsterdam, 1978), Vol. 1, Chap. 3.
[7] I. Felner and I. Nowik, J. Phys. Chem. Solids **39**, 767 (1978).
[8] Z. Islam, C. Detlefs, C. Song, A. I. Goldman, V. Antropov, B. N. Harmon, S. L. Bud'ko, T. Wiener, P. C. Canfield, D. Wermeille, and K. D. Finkelstein, Phys. Rev. Lett. **83**, 2817 (1999).
[9] O. K. Andersen, Phys. Rev. B **12**, 3060 (1975).
[10] O. K. Andersen, O. Jepsen, and D. Glötzel, in *Highlights of Condensed-Matter Theory*, edited by F. Bassani, F. Fumi, and M. P. Tosi (North-Holland, Amsterdam, 1985), pp. 59–176.
[11] H. L. Skriver, *The LMTO Method:Muffin-Tin Orbitals and Electronic Structure* (Springer-Verlag, Berlin, 1984).
[12] W. Rieger and E. Parthé, Monatsch. Chem. **100**, 444 (1969).
[13] P. C. Canfield and Z. Fisk, Philos. Mag. B **56**, 1117 (1992).
[14] C. G. Olson, Nucl. Instrum. Methods Phys. Res. A **266**, 205 (1988).
[15] F. J. Himpsel, Adv. Phys. **32**, 1 (1983).
[16] L. I. Johansson and C. G. Larsson, in *Angle-Resolved Photoemission*, edited by S. D. Kevan (Elsevier, Amsterdam, 1992), Chap. 6.
[17] J. Stöhr, P. S. Wehner, R. S. Williams, G. Apai, and D. A. Shirley, Phys. Rev. B **17**, 587 (1978).
[18] Z. Islam, Ph.D. thesis, Iowa State University, 1999 (unpublished).
[19] W. E. Spicer, in *Band Structure Spectroscopy of Metals and Alloys*, edited by D. J. Fabian and L. M. Watson (Academic Press, London, 1973).
[20] S. Hüfner, in *Photoemission in Solids II*, edited by L. Ley and M. Cardona (Springer-Verlag, Berlin, 1979).
[21] D. W. Lynch and C. G. Olson, *Photoemission Studies of High-Temperature Superconductors* (Cambridge University Press, Cambridge, 1999), p. 245.
[22] R. Liu, B. W. Veal, A. P. Paulikas, J. W. Downey, P. J. Kostic, S. Fleshler, U. Welp, C. G. Olson, X. Wu, A. J. Arko, and J. J. Joyce, Phys. Rev. B **46**, 11056 (1992).
[23] W. Eberhardt and E. W. Plummer, Phys. Rev. B **21**, 3245 (1980).
[24] E. W. Plummer and W. Eberhardt, Adv. Chem. Phys. **49**, 533 (1982).